Microstructural Changes during Overtempering of High-Speed Steels

S. KARAGÖZ, H.F. FISCHMEISTER, H.-O. ANDRÉN, and CAI GUANG-JUN

To elucidate the mechanisms determining the creep resistance of high-speed steels during tool service, overtempering at 600 °C has been investigated for two alloys modeling the matrix compositions of AISI M2 and T1. Composition changes and coarsening of the secondary hardening precipitates were studied by transmission electron microscopy and field-ion microscopy with atom probe analysis. Strengthening in the peak-hardened state is due to coherent precipitates of types M_2C and MC. During overtempering, M_2C coarsens too rapidly to be of importance for the sustained strength of the material. The MC precipitates, on the other hand, are fairly stable. Some coarsening does occur, but the MC population is replenished by a second wave of precipitation which makes use of the roughly 50 pct of carbide-forming elements, carbon, and nitrogen, which remained in solid solution after tempering to the peak-hardened state. This precipitation reaction continues for times of the order of the tool life.

I. INTRODUCTION

THE high-speed steels are among the strongest and most wear-resistant iron-based alloys known. Their martensitic matrix is strengthened by secondary hardening, which produces fine, coherent precipitates[1] of types MC and M_2C. These precipitates are of the order of a few up to some tens of nanometers in size. Atom probe analysis in the field ion microscope of a wide range of alloys has shown that both types of precipitate contain (Fe + Cr) and (Mo + W) roughly in the ratio 1:1, the elements in each pair being mutually exchangeable to a large extent.[2] A characteristic difference between the two types of precipitates concerns their vanadium content, which is about 30 at. pct in the MC particles and only half as much in the M_2C phase.[2 8] Enclosed in the precipitate-strengthened matrix are large ("blocky") carbides, of the order of 1 to 10 μm, which have remained undissolved during austenitization. They are important for the wear resistance of the steels, but they are not affected by the overtempering process.

For satisfactory service in metal cutting, the matrix must be strong enough to keep the blocky carbides in place and to prevent blunting of the tool edge by plastic flow or creep. During operation, a large portion of the tool is heated to temperatures above that of the secondary hardening treatment (typically 550 °C). At moderate cutting speeds, the temperature field around the cutting edge has a local peak at 700 °C, not at the edge itself, but at the point of maximum frictional contact between the chip and the tool. This is due to the fact that the work material acts as a large volume heat sink.[9] To understand tool performance, the behavior of the precipitate population at temperatures between 550 °C and 700 °C is of interest.

The composition of the secondary hardening precipitates is fairly well known from atom probe field ion microscopy (APFIM) work,[2,5-8] but only in the state of peak hardness after tempering at 550 °C. Little is known about their fate during overheating at typical service temperatures. Strong overtempering was used to facilitate the study of the carbide precipitates in Kuo's classical work by X-ray diffraction[10,11] and, similarly, in early studies by transmission electron microscopy (TEM).[12,13] The temperature dependence of carbide precipitation and coarsening has been studied systematically by TEM for model alloys of Fe-C with W, Mo, or V added singly or in simple combinations,[14,15,16] and there are also studies of isothermal overtempering of such steels.[17,18] However, the processes occurring in actual (multicomponent) high-speed tool steels during long heating in the range of service temperatures have not been studied by modern analytical methods, with the single exception of some results on overtempering at 700 °C in Reference 5 and recent work in one of our groups.[19] At 700 °C, the alloys soften in a matter of minutes. Therefore, the overtempering process was studied at a less extreme temperature, 600 °C, where softening is slow enough to allow comparisons with practical service lives.

Many metal cutting operations involve cyclic loading, and in these cases, high-temperature fatigue strength may be of equal or even greater importance than the static hot strength of the matrix. Other mechanisms which may become important in certain tooling applications are related to the weakening of internal boundaries by impurity segregation or carbide precipitation. In this article, we direct our attention exclusively to the hot strength of the matrix, which we consider to be a basic factor in all tool applications, especially in uninterrupted cutting.

II. EXPERIMENTAL

Two archetypal high-speed tool steels, AISI M2 and AISI T1, were selected for this study. Their nominal

S. KARAGÖZ, Professor, Department of Metallurgy, Yildiz University, Istanbul, Turkey, is Humboldt Research Fellow on leave of absence at Max-Planck-Institut für Metallforschung, Stuttgart. H.F. FISCHMEISTER, Fellow ASM, is Professor of Metallurgy, University of Stuttgart, and Director, Max-Planck-Institut für Metallforschung, D-7000 Stuttgart 1, Germany. H.-O. ANDRÉN, Associate Professor, and CAI GUANG-JUN, Research Student, are with the Department of Physics, Chalmers University of Technology, S-41296 Gotenburg, Sweden.

Manuscript submitted July 11, 1991.

compositions are given in Table I. Atom probe field ion microscopy and TEM were used to study the behavior of the secondary hardening precipitates during isothermal annealing at 600 °C.

Field ion microscope specimens have the form of thin needles. They must have a smooth surface to survive the intense mechanical stress which arises when the field is pulsed to remove surface atoms for analysis in the atom probe. Blocky carbides cause surface roughness during the preparation of the specimens, and a large percentage of the needles may be broken halfway during analysis. To avoid this, the APFIM specimens were prepared from special alloys made to the composition of the matrix that encloses the blocky carbides in the actual tool materials and which are thus free of blocky carbides; the matrix compositions are known from earlier studies.[20,21] These alloys will be termed matrix model alloys, M(M2) and M(T1); their compositions and those of similar alloys used in earlier work[2] are stated in Table I. The alloys were induction melted in the form of 20-kg ingots of 110 × 110 mm^2 section size and hot-worked to 20 × 20 mm^2 bars. Specimens of 10 × 20 × 20 mm^3 were cut from these bars after soft annealing. The specimens were given the heat treatment that is usual for the tool steels they represent: austenitizing at 1200 °C for M(M2) and at 1240 °C for M(T1), followed by quenching and triple tempering for 60 minutes at 550 °C for both alloys. The resulting hardness was 63 HRC = 815 HV_{10} for M(M2) and 60 HRC = 725 HV_{10} for M(T1). These values are below those of the actual tool steels in the peak hardened state because the hardness contribution of the blocky carbides is missing.

After the standard triple tempering treatment at 550 °C, the alloys were isothermally overtempered at 600 °C. Specimens for analysis by APFIM and TEM were prepared in the normal way.[4] The energy-compensated APFIM instrument used, as well as the APFIM procedure, have been described elsewhere.[2,22,23] To obtain statistically significant results, all precipitates in the FIM image were analyzed. Those large enough were also analyzed by scanning transmission electron microscopy with energy-dispersive X-ray analysis (STEM-EDX).

The microstructural investigation was complemented by hardness measurements after different times of overtempering. The measurements were made using a Vickers diamond indenter in a Zwick 3212B Universal Hardness Tester, following standard procedure as laid down in the German standard DIN 50133, with a load of 98.1 N (= 10 kg, as signified by the symbol HV_{10}). Hardness values reported in this article are the mean of five measurements. In addition, the change of electrical resistivity during overtempering was measured, using cylindrical specimens of 5-mm diameter and 30-mm length in a four-contact arrangement with a Keithley 228 precision current supply and a Keithley 181 nanovoltmeter, with a precision better than 0.02 pct.

III. RESULTS

A remark about nomenclature must be made before presenting the results. In the context of this article, the meaning of the term "matrix" depends on the level of image resolution. The matrix model alloys represent the matrix found between the blocky carbides in the actual tool materials. In this statement, the term matrix is used in a "macroscopic" sense, *i.e.*, on the resolution level of the optical microscope, as is customary in the tool steel literature. The chemical composition of this (macroscopic) matrix includes the secondary hardening precipitates.

On the resolution level of FIM, we study the matrix found between the secondary hardening precipitates. Its composition excludes the contribution of these particles. To avoid signal contributions from the precipitates in determining the composition of this (microscopic) matrix, the APFIM probe spot had to be moved, slalom fashion, between them.

The effect of overtempering at 600 °C on the hardness of the triple tempered matrix model alloys is shown in Figure 1. Up to 100 minutes, there is no significant loss of hardness (and, as will be shown, no significant change in microstructure). However, the electrical resistivity data presented in Figure 2 indicate that some changes are taking place in the material. The onset of softening after 100 minutes is paralleled, approximately, by a change in the rate of the resistivity drop between 100 and 300 minutes. Even the crossover of the hardness curves of alloys M(M2) and M(T1) at about 700 minutes of overtempering is duplicated (at somewhat longer times) in the resistivity curves.

As originally tempered at 550 °C, both matrix model

Table I. Compositions of Steels Studied

	C	W	Mo	V	Cr	Fe
Tool steel grades:						
AISI M2 (nominal), weight percent	0.9	6	5	2	4	bal.
AISI T1 (nominal), weight percent	0.8	18	—	1	4	bal.
Matrix model alloys:						
M(M2), weight percent	0.55	3.93	3.57	0.99	4.63	bal.
M(M2), atomic percent	2.60	1.22	2.12	1.10	5.06	bal.
M(T1), weight percent	0.44	7.29	0.55	0.69	4.11	bal.
M(T1), atomic percent	2.12	2.29	0.33	0.78	4.57	bal.
Earlier matrix model alloys:[2]						
M(M2), atomic percent	2.9	1.2	2.1	1.1	4.6	bal.
M(T1), atomic percent	2.2	2.3	0.2	0.7	4.3	bal.

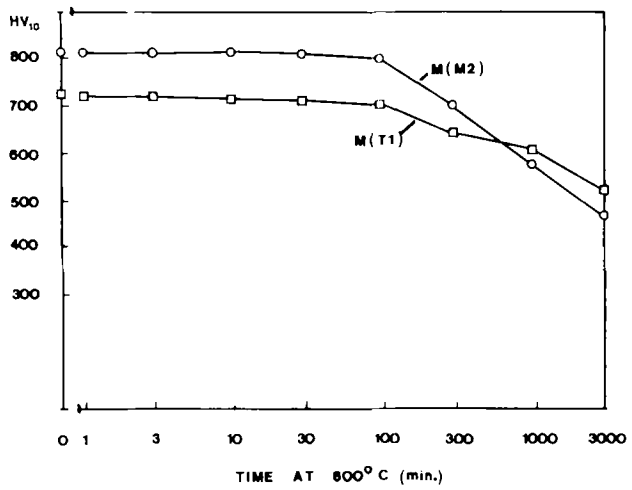

Fig. 1 — Effect of overtempering at 600 °C on the hardness (measured at room temperature) of HSS matrix model alloys M(M2) and M(T1).

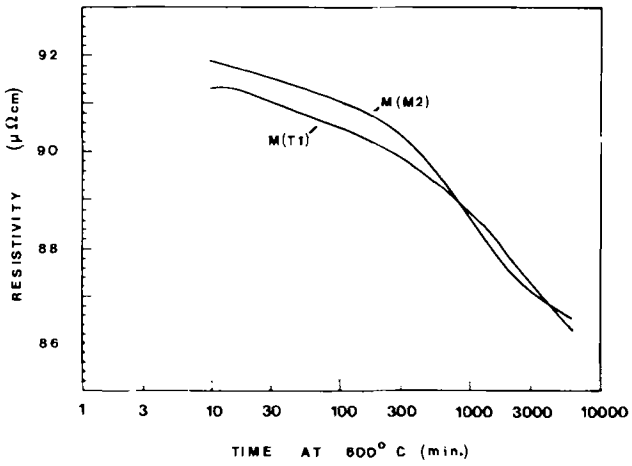

Fig. 2 — Effect of overtempering at 600 °C on the electrical resistivity (measured at temperature) of HSS matrix model alloys M(M2) and M(T1).

alloys consist predominantly of lath martensite (Figure 3). In accordance with its lower carbon content, alloy M(T1) has a lower fraction of plate martensite (approximately 10 pct) than alloy M(M2) (approximately 20 pct). Transmission electron microscopy images (Figure 4) of overtempered specimens clearly show the MC carbides but not the M_2C carbides, whose weak and streaky reflections are too close to those of MC for selective dark-field imaging. Only at overtempering periods between 1000 and 3000 minutes, when the size of the M_2C particles increases dramatically, do these precipitates become clearly discernable in TEM (Figure 5). M_3C carbides are found at the lath boundaries (Figure 6) in both alloys at early stages of overtempering, but they disappear at times beyond 100 minutes.

After the longest overtempering periods, small amounts of M_7C_3 could be identified in both materials (Table II). Their morphology was different from the MC and M_2C precipitates, and their size was larger. These coarse precipitates point toward an incipient approach to equilibrium, but they will not influence the strengthening of the

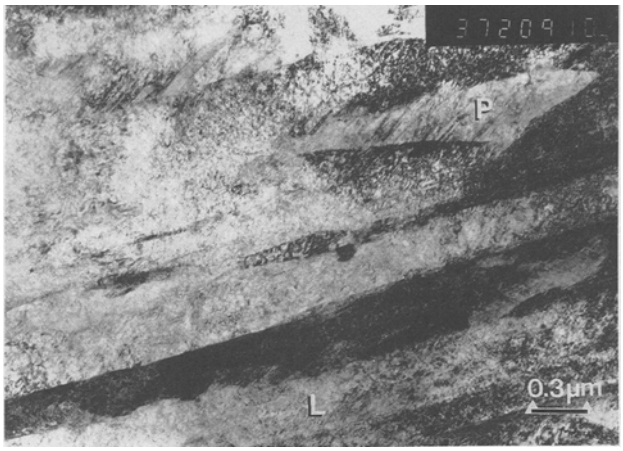

Fig. 3 — TEM micrograph of alloy M(M2): lath martensite (L) with small amounts of plate martensite (P).

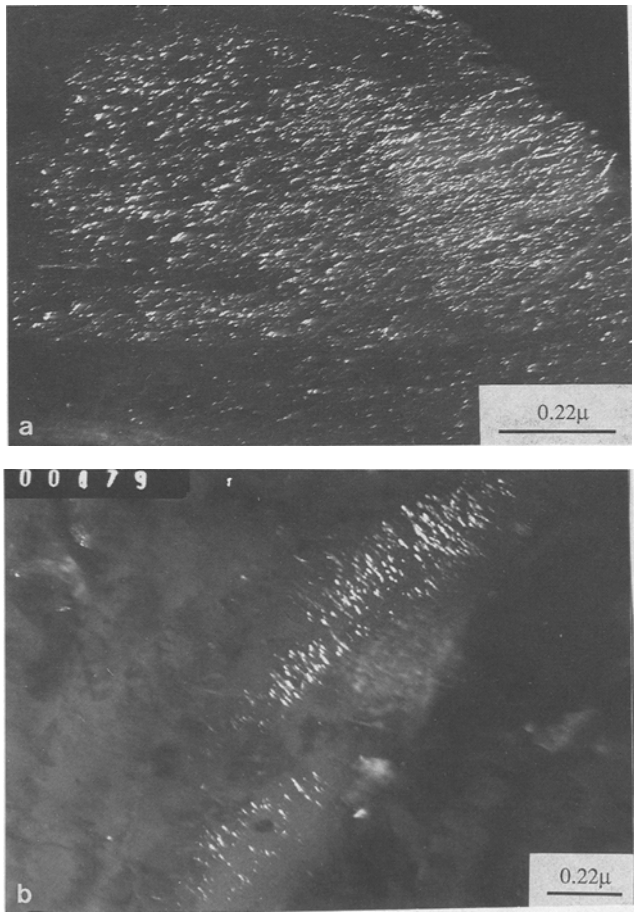

Fig. 4 — MC carbides in alloy M(M2). TEM dark-field images using $(111)_{MC}$ reflection: (*a*) 100 min and (*b*) 3000 min at 600 °C.

matrix and are therefore of secondary interest in the present context. They may, however, embrittle the material, being mostly situated at internal boundaries, and this may affect tool performance in interrupted cutting.

Figure 7 illustrates the changes in the precipitate distribution of alloy M(M2) as seen in the field ion microscope. In the original peak hardened state and for the

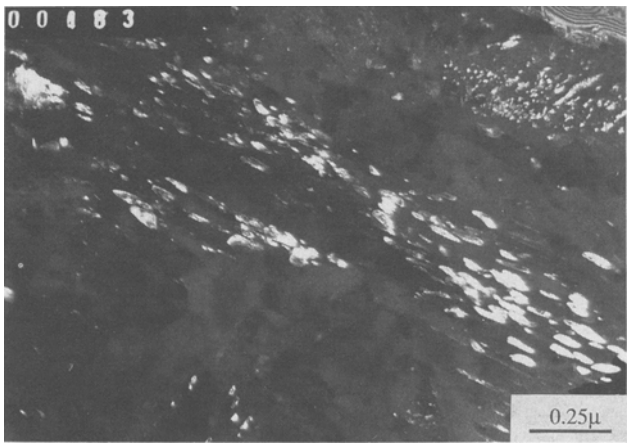

Fig. 5—Coarsened M_2C carbides at a lath boundary in alloy M(M2) after 3000 min at 600 °C. TEM dark-field image using $(1\bar{1}01)_{M_2C}$ reflection.

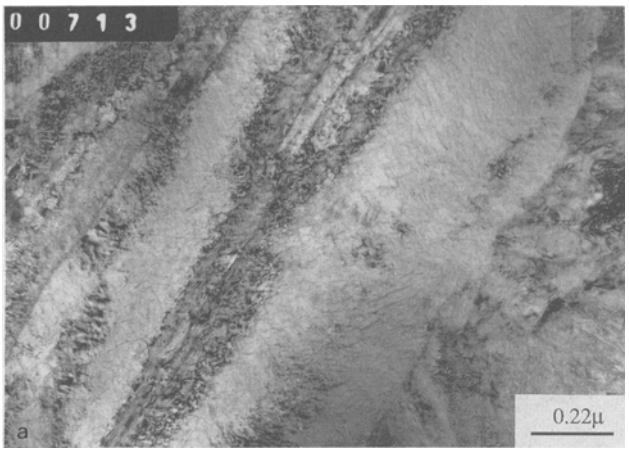

Fig. 6—M_3C carbides at a lath boundary in alloy M(M2) after 100 min at 600 °C. (*a*) TEM, bright-field image and (*b*) TEM dark-field image using $(020)_{M_3C}$ reflection.

first 100 minutes of overtempering (Figure 7(a)), the interior of the laths contains a dense distribution of precipitates, which are presumably situated on dislocations. The lath boundaries are even more densely populated. During overtempering, the boundary precipitates become coarser and more numerous, until thick bands of agglomerated particles are formed at the boundaries (Figure 7(b)). In the final stage, the coarsening of the boundary precipitates has progressed to such a degree that the boundaries are no longer continuously decorated, and strong coarsening has reduced the number of precipitates in the interior of the laths (Figure 7(c)). Note that this reduction of the number density of intra-lath precipitates occurs in the stage in which the hardness starts to drop significantly: at 100 minutes (Figure 7(b)), the precipitate density within the laths is still as high as initially, and in some places even higher; at 300 minutes, it has begun to decrease.

An attempt has been made to quantify typical particle dimensions and number densities at various stages of overtempering by TEM, and the results are collected in Table II. In agreement with the qualitative observations by FIM, the number density of the MC particles seems to pass through a maximum at 100 minutes for alloy M(M2) and at 300 minutes for M(T1). Note that the lack of data for M_2C at short and intermediate times in Table II does not mean that such carbides are completely absent: for the reasons stated previously, they can be detected only by FIM. In our earlier work on precipitates in the peak hardened state in M(M2),[2] the number densities of M_2C and MC were in the ratio of 70:30. Overtempering at first produces the dense boundary aggregates shown in Figure 7, which consist mainly of M_2C with a small admixture of MC. Prolonged overtempering then coarsens the M_2C particles so strongly that finally their number density falls below that of the more slowly coarsening MC precipitates (Table II).

In alloy M(T1), the coarsening process seems to progress in a similar fashion, although at all stages, the lath boundaries are less strongly decorated than in M(M2) (Figure 8). However, the kinetics differ. In spite of the low V content of M(T1), the initial population density of MC is higher in M(T1), on an absolute scale, than in M(M2). In the peak hardened state,[2] MC particles were preponderant over M_2C in the ratio 60:40, in contrast to M(M2). This may be related to the fact that the MC particles in M(T1) are especially rich in Cr, which, as discussed elsewhere,[2] reduces the lattice misfit and lowers the nucleation threshold. On the other hand, the formation of M_2C is hindered in M(T1) by the lack of the preferred M_2C former, Mo,[2] and the slower diffusion rate of W.[15] As in M(M2), the MC population in M(T1) increases at early stages of overtempering and then passes through a maximum, but this occurs later than in M(M2). Long overtempering coarsens the M_2C particles in a similar manner as in M(M2) so that at 3000 minutes, the number density of M_2C is much lower than that of MC. At this late stage, in fact, both alloys show quite similar number densities for each precipitate type.

The composition of the precipitates was analyzed by APFIM. The results are collected in Table III and are illustrated for the case of M_2C in Figure 9. The large

Table II. Typical Size, Density, and Distribution of the Secondary Hardening Carbides in the Overtempered State

Alloy	Treatment	Precipitate Type	Density (10^{15}/cm^3)	Size (nm)	Distribution
M(M2)	600 °C/1 min	MC	96	8 × 3	inside lath
		M_3C			continuous along lath boundaries
	600 °C/100 min	MC	106	13 × 2	inside lath
		M_3C			continuous along lath boundaries
	600 °C/300 min	MC	85	15 × 2	inside lath
	600 °C/3000 min	MC	40	21 × 6	inside lath
		M_2C	2	90 × 24	inside lath and along lath boundaries
		M_7C_3	very few	100 × 60	at grain boundaries
M(T1)	600 °C/1 min	MC	few	very fine	inside lath
		M_3C		400 × 75	inside lath
	600 °C/100 min	MC	38	15 × 2	inside lath
		M_3C		150 × 60	inside lath
	600 °C/300 min	MC	78	15 × 2	inside lath
	600 °C/3000 min	MC	47	17 × 4	inside lath
		M_2C	2	100 × 30	inside lath and along lath boundaries
		M_7C_3	very few	400 × 30	at lath boundaries

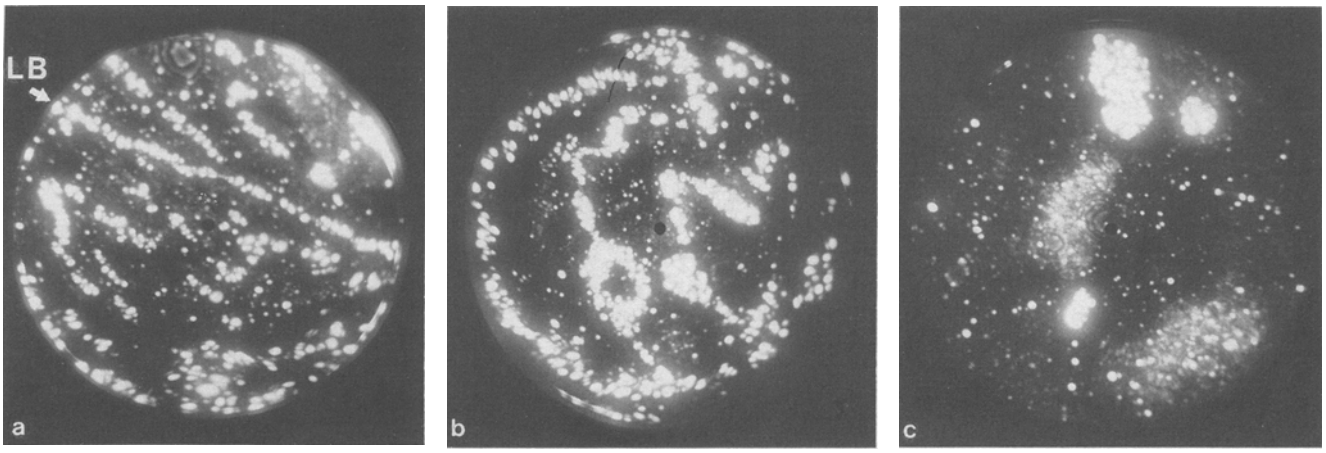

Fig. 7 — Field ion micrographs illustrating the coarsening of the secondary hardening precipitates in alloy M(M2); LB = lath boundary: (*a*) after 100 min at 600 °C, field of view ≈160 nm; (*b*) after 300 min at 600 °C, field of view ≈190 nm; and (*c*) after 3000 min at 600 °C, field of view ≈160 nm.

M_2C particles obtained after 3000 minutes of overtempering could be analyzed both by APFIM and by STEM-EDX, using extraction replicas to preclude signal contributions from the matrix. The two sets of data are compared in Figure 9. Carbide compositions at peak hardness, taken from our earlier APFIM measurements,[21] are included in Table III for comparison. Taking into account the difference in alloy composition in the earlier and in the present work (in particular, the present alloy M(M2) had a significantly higher Cr content than the one used earlier; Table I), the agreement with the present values at short overtempering times is satisfactory for MC and quite good for M_2C.

The scatter of the APFIM results at 3000 minutes of overtempering (Figure 9) is believed to reflect true variations among individual particles, since the precipitates analyzed in APFIM were large enough to preclude spurious matrix contributions or large errors due to counting statistics. The M_2C phase is, in fact, known to have a wide range of solubility with respect to its various metallic components.[24,25] The STEM-EDX data fall within the range of the APFIM data, with the exception of Cr. Note that the error bars shown in the figure represent one standard deviation only.

Fewer measurements were made for the MC precipitates (Table III), and being based on lower total counts, their reliability is inferior to that of the M_2C data. This may explain the poorer agreement of the present data for short periods of overtempering with those for the peak hardened state from our earlier measurements, which are included in Table III. The data suggest a trend for the W content of the MC precipitates, which is remarkably low initially and after short times of overtempering, to increase during prolonged overtempering. Beyond this trend, no conclusions seem justified concerning compositional changes during overtempering.

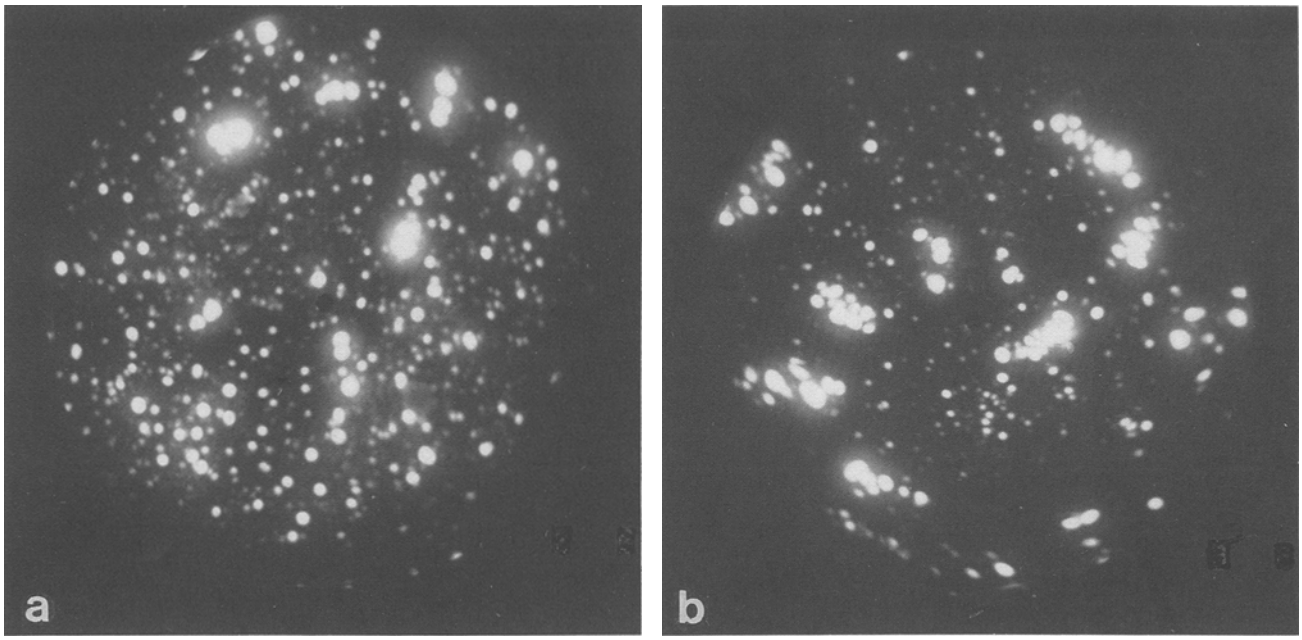

Fig. 8—Field ion micrographs illustrating the coarsening of the secondary hardening precipitates in alloy M(T1): (*a*) after 1 min at 600 °C, field of view ≈145 nm and (*b*) after 300 min at 600 °C, field of view ≈110 nm.

Table III. Compositions of Carbide Precipitates in the Matrix Model Alloys M(M2) and M(T1) as Determined by APFIM and STEM-EDX*

Treatment	Total Count**	Cr	V	Mo	W	Fe	Stoichiometry
(a) Precipitate Compositions Determined in Alloy M(M2) by APFIM (Atomic Percent)							
MC							
3 × 550 °C[2]	237	17.0	36.4	41.8	4.8	—	$MC_{1.09}$
600 °C/100 min	123	29.9	32.8	35.8	1.5	—	$MC_{0.84}$
600 °C/300 min	443	22.9	28.8	36.0	12.3	—	$MC_{0.88}$
M_2C							
3 × 550 °C[2]	777	30.5	15.9	45.4	8.2	—	$M_2C_{1.10}$
600 °C/100 min	694	30.6	18.8	38.5	12.1	—	$M_2C_{1.10}$
600 °C/300 min	1963	26.6	21.7	39.2	12.5	—	$M_2C_{1.03}$
600 °C/3000 min	889	24.1	8.5	49.6	16.0	1.8	$M_2C_{0.90}$
600 °C/3000 min (STEM-EDX)	—	31.3	11.0	39.1	16.1	2.5	ND
M_3C							
600 °C/100 min	804	39.9	6.4	19.1	5.9	28.7	$M_3C_{1.07}$
(b) Precipitate Compositions Determined in Alloy M(T1) by APFIM (Atomic Percent)							
MC							
3 × 550 °C[2]	293	47.6	35.0	16.6	0.8	—	$MC_{0.80}$
600 °C/300 min	113	34.5	37.9	10.4	17.2	—	$MC_{0.95}$
M_2C							
3 × 550 °C[2]	407	53.7	16.2	7.2	22.9	—	$M_2C_{0.79}$
600 °C/1 min	121	39.5	19.8	11.8	28.9	—	$M_2C_{0.87}$
600 °C/300 min	645	42.6	23.9	7.5	26.0	—	$M_2C_{1.05}$

*Compositions are given in atomic percent normalized to Σ metal = 100; carbon stoichiometry is stated separately.
**"Total count" = total number of atoms recorded, usually from several particles.

M_3C precipitates are poorly visible in the field ion microscope and not numerous. Therefore, it was not possible to analyze their compositions except in the single case stated in Table III.

The carbide compositions presented in Table III pertain to particles which were large enough to be analyzed as separate entities. In addition to these, the field ion micrographs show a general background of very small particles (Figures 7 and 8). Their main constituents can be identified by studying the sequence of arrival of different species in the atom probe detector from a stationary image spot located between the larger carbides. Such

a sequence is illustrated, in the form of a "ladder diagram," in Figure 10. The particles can be correlated with the arrival of C, N, Cr, V, Mo, and W atoms which are not accompanied by proportional amounts of iron, as they would be in the homogeneous matrix. Analysis of the ladder diagrams indicates that the small particles are carbides or carbonitrides containing predominantly Cr, with some V and Mo, and only occasionally some W. They are rich in C and should be considered as MC rather than M_2C. Their dimensions can be derived from the lengths of the plateaus of the Fe signal in the ladder diagram. Using the lattice constant of MC (4.3 Å), we obtain particle diameters of the order of 1.3 nm after 300 minutes of overtempering and of 1.5 nm after 1000 minutes in the case of alloy M(M2).

Dark-field micrographs of the type shown in Figure 4(a) actually show very weak extra contrast effects (not visible in the reproduction) besides those of the larger secondary hardening carbides. These extra contrast effects can be correlated with the fine particles discussed here.

Surprisingly, the number density of these very fine particles, as derived from TEM and FIM images, is found to increase with time up to 1000 minutes at 600 °C. After 3000 minutes, however, the fine particles have virtually disappeared. This time dependence indicates that the fine particles are not formed during cooling from the overtempering anneal. Instead, we consider them to be the result of a second wave of precipitation occurring in the wake of the coarsening of the original secondary hardening precipitates.

We now turn to the composition changes in the matrix. They are shown in Figure 11 for alloy M(M2). A marked depletion of Cr is noted by the end of the first 100 minutes, while the contents of carbon and metallic alloy elements have remained largely unaffected. At times beyond 100 minutes, when the hardness drop becomes pronounced, both carbon and metallic alloy elements decrease in the matrix. Obviously, the formation of the large carbides which now appear involves consumption of residual solute and is not merely an Ostwald ripening process. Alloy M(T1) shows the same tendency, as can be seen in Table IV.

The APFIM values for carbon in the matrix are far in excess of the equilibrium solubility in the Fe-C binary at 600 °C and also of the corresponding value in the six-component system Fe-Cr-Mo-W-V-C, as indicated by recent thermodynamical equilibrium calculations.[26] As mentioned above, carbon often appears in the atom probe spectra in the form of C_2^+ or of higher molecular ions,

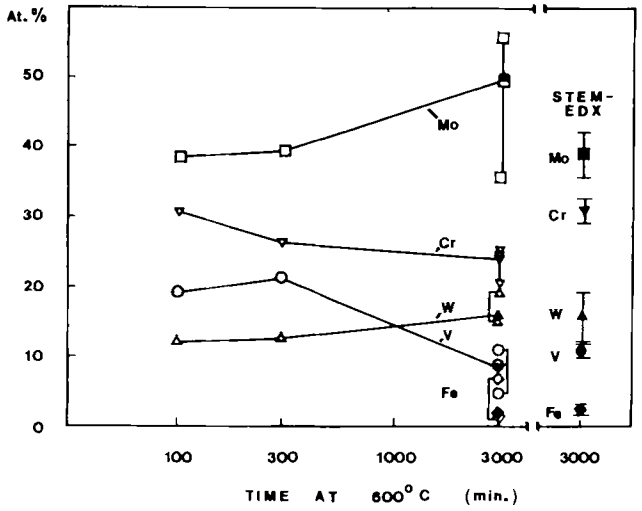

Fig. 9—Composition of M_2C precipitates in alloy M(M2) during overtempering at 600 °C (APFIM and STEM-EDX measurements). At 3000 min, APFIM measurements on three individual particles (with dark symbols signifying count-weighted averages) are compared to STEM-EDX measurements on 16 particles; the error bars for the latter correspond to the standard deviation.

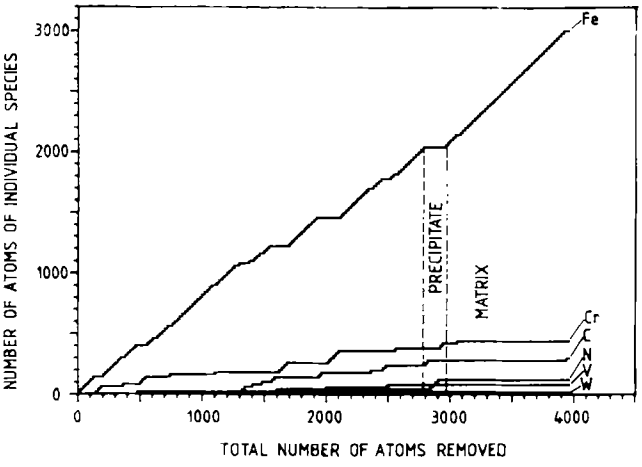

Fig. 10—Ladder diagram of M(M2) after 1000 min at 600 °C.

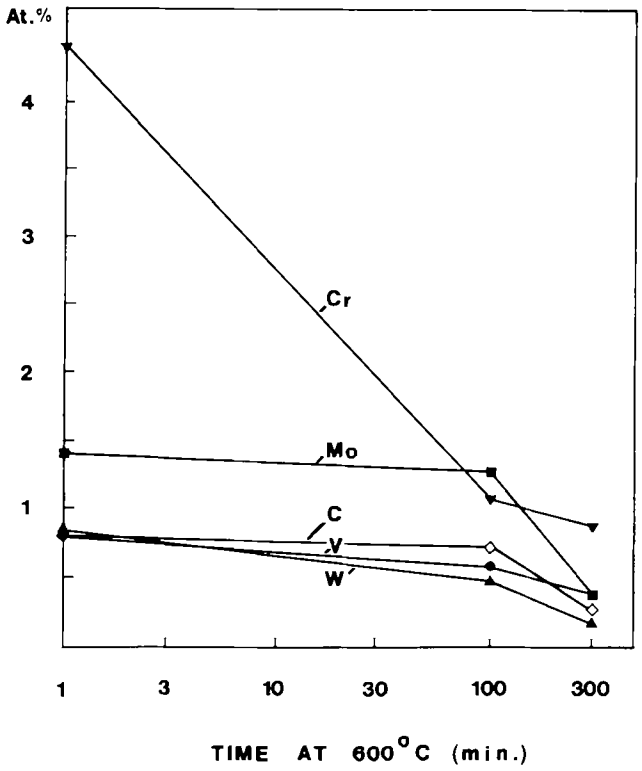

Fig. 11—Compositional changes in the matrix of alloy M(M2) during overtempering at 600 °C.

Table IV. Compositions of Matrices of Alloys M(M2) and M(T1) (Atomic Percent)

Treatment	C	W	Mo	V	Cr	Fe
M(M2)						
3 × 550 °C[2]	1.5	0.3	1.3	0.6	3.5	bal.
600 °C/1 min	0.8	0.85	1.4	0.8	4.4	bal.
600 °C/100 min*	0.76 ± 0.3	0.5 ± 0.25	1.3 ± 0.4	0.6 ± 0.3	1.1 ± 0.5	bal.
600 °C/300 min	0.3	0.2	0.4	0.4	0.9	bal.
M(T1)						
3 × 550 °C[2]	0.4	1.4	ND	ND	2.1	bal.
600 °C/1 min	1.7	1.9	0.3	0.3	3.6	bal.
600 °C/300 min	0.5	1.0	0.15	0.15	2.5	bal.

*With standard deviation.

indicating the existence of carbon-rich clusters of a size below the resolution of the APFIM analysis. Such clusters may be assumed to be located on the very dense dislocation network which exists in the specimens.

IV. DISCUSSION

Older observations about carbides forming during overtempering of high-speed steels have been reviewed by Kupalova[27] and Mukherjee.[28] Many of these observations were based on X-ray diffraction or replica electron microscopy, which cannot detect the small precipitates responsible for secondary hardening. They must be considered characteristic of more intensely overtempered specimens than those which concern us here. On the whole, these studies indicate that M_7C_3, $M_{23}C_6$, and M_6C tend to form mainly at temperatures above that of our present study. In alloy T1, M_7C_3 seems to form more readily than in alloy M2; we believe this to be related to the higher content of vanadium in alloy M2, and also to a propensity of plate martensite (in alloy M2) to favor the nucleation of M_3C rather than M_7C_3.[29] More recently, thin foil electron microscopy studies have been published which deal with powder metallurgy processed M2 and its carbide-enriched descendents ASP 23, 30, and 60 at 700 °C[5] and at 600 °C.[19] Neither of these articles reports any M_7C_3, except at times as long as 100 hours at 560 °C in ASP 60.[5] After 24 hours at 600 °C, the study of Wang *et al.*[19] showed coarse particles of M_3C, $M_{23}C_6$, and M_6C surrounded by zones of depletion of the MC and M_2C dispersion. In our material, the coarse M_3C particles were also found but no M_6C and $M_{23}C_6$. We have no conclusive explanation for this difference, but since our specimens had a much lower carbon content, we feel that the difference might again be related to different nucleation effects in plate and lath martensites (the M_6C and $M_{23}C_6$ particles often sit on plate and twin boundaries), and to the lack, in our alloys, of blocky carbides which have been demonstrated[30] to serve as nucleation sites for $M_{23}C_6$. In the present context, where our main concern is the creep strengthening, the minority precipitate phases discussed above are of secondary interest.

Turning now to the matrix, the rapid depletion of chromium shown in Figure 11 invites discussion. Transmission electron microscopy does not show the formation of any new carbide phases at this stage. Since the Cr depletion is not accompanied by a decrease of carbon, it cannot be caused by the formation of additional amounts of carbide. Instead, we must assume that the chromium is absorbed by compositional changes in an already existing carbide phase. A plausible candidate is Fe_3C, which is present at grain boundaries at the beginning of overtempering in TEM studies[19] and which has also been found here (Table II). In the present study, continuous bands of M_3C at the lath boundaries could be observed by TEM but not by APFIM. This suggests that the M_3C was rich in Fe and poor in Cr: because of the lower bonding energy of iron-rich carbides, field evaporation in the FIM will not bring the Fe_3C particles to stand proud of the matrix as readily as the more stable alloy carbides, keeping their FIM contrast poor.

In a TEM study of the tempering of tungsten steels at 700 °C, Davenport and Honeycombe[15] have suggested the occurrence of two transformation sequences,

$$Fe_3C \Rightarrow M_2C \Rightarrow M_6C$$

and

$$Fe_3C \Rightarrow M_{23}C_6 \Rightarrow M_6C$$

They emphasize that the transformations seem to occur *in situ*, but that the $M_{23}C_6$ might, in fact, be formed by nucleation at the cementite/ferrite interface. In this light, our present findings could be interpreted as a process of nucleation of Cr-rich $M_{23}C_6$ on the surfaces of cementite precipitates at internal martensite boundaries, accompanied by a conversion of the Fe_3C to $(Fe,Cr)_3C$ and then to $M_{23}C_6$. Since carbon would be supplied by the conversion process itself (seeing that M_3C contains more carbon per metal atom than $M_{23}C_6$), such a reaction would consume Cr without lowering the carbon level in the matrix. Kuo[31] reports a maximum solubility of approximately 18 at. pct for Cr in Fe_3C. In the present work, a Cr content as high as 40 at. pct was measured for an apparent M_3C particle in M(M2) (Table III). This could have been an intermediate state in the transformation of an Fe_3C particle with a reaction layer of $M_{23}C_6$.

We note in passing that the absorption of a substantial fraction of solute Cr from the matrix into an existing carbide phase would account for the drop in resistivity during the first 100 minutes, which is not accompanied by noticeable changes in microstructure or hardness.

Figure 9 shows the compositional changes of the M_2C precipitates during coarsening. Without neglecting the

scatter and the differences in the absolute levels of the APFIM and the STEM-EDX measurements, the trends shown by the APFIM data appear plausible. The upward trend of Mo and W, and the downward trend of V and Cr which is suggested by Figure 9, would fit a gradual shift of the particle composition from M_2C toward M_6C. The latter carbide can accommodate large amounts of Mo and W but has much less solubility for V than M_2C[25] and a smaller solubility for Cr.[24,32] M_6C is also the phase following M_2C in the transformation sequence reported by Davenport and Honeycombe.[15]

From the point of view of service properties, we want to know which precipitates are responsible for sustaining the creep strength of the matrix during service. The M_2C particles coarsen too rapidly to fill this role. For the MC particles produced in the initial tempering treatment, the TEM results indicate an increase in number density up to 100 minutes in M(M2) and up to 300 minutes in M(T1). Field ion microscopy observations indicate that the remaining solutes form additional, very fine M(C, N) particles during a second wave of precipitation. Their number density continues to increase up to 1000 minutes at 600 °C. The slowness of this reaction may be connected with the different chemistry of these precipitates.

In earlier work on the relation between chemical composition, microstructure, and cutting performance of high-speed steels,[7,33] we have emphasized that the observed correlations cannot be explained without assuming that pinning centers lost by coarsening of the tempering carbides are continually replaced during service. This postulate was based, in part, on reported TEM observations of continued precipitation during creep of austenitic high-temperature chromium steels,[34,35,36] to which analogous observations by APFIM on a ferritic chromium steel have been added recently.[37,38] The hypothesis that such a process occurs in high-speed steels as well is supported by our observation that the initial tempering reaction consumes only about one-half of the carbide-forming solutes[2] and by the present finding of a second wave of precipitates formed from the remaining solutes. Being homogeneously distributed within the martensite laths, these fine precipitates will replace pinning centers lost by the coarsening of the older precipitates. In a cutting edge, which undergoes slow plastic deformation, such precipitates will be especially efficient if they immobilize the newly formed dislocation segments. This has been observed in the high-temperature chromium steels mentioned earlier. Conversely, newly formed dislocations would provide favorable nucleation sites throughout the service life. No systematic measurements of dislocation density were made in the present work, but in qualitative terms, the dislocation density remained high during overtempering, similar to what has been reported in earlier TEM studies of the overtempering of high-speed steel matrices.[15,16] One of these studies, in fact, emphasizes the role of MC precipitates in stabilizing the dislocation network.[15]

V. CONCLUSIONS

Overtempering at 600 °C produces the following changes in the population of secondary hardening precipitates in the matrices of high-speed steels of types AISI M2 and T1:

M_3C, which is found in the form of relatively large boundary precipitates in the peak hardened state (before overtempering), is originally Fe-rich, as indicated by its contrast in FIM and TEM images. It is concluded that this carbide gradually picks up Cr from the residual solute in the matrix, and it is suggested that the incorporation of Cr occurs in the process of a conversion from M_3C to $M_{23}C_6$.

M_2C seems to give the main hardness contribution in the initial peak hardened state. During overtempering, the ratio of (Cr + V) to (Mo + W) in the M_2C precipitates changes in the direction toward M_6C. The particles coarsen rapidly, and therefore, this precipitate cannot be responsible for the remarkable long-time strength exhibited by the steels at 600 °C.

MC survives much longer in the form of a fine, homogeneous precipitate distribution. Its number density actually increases during the first 1000 minutes of overtempering at 600 °C, thanks to a second wave of precipitation which is more sluggish than that which occurs during ordinary tempering and which involves some nitrogen besides carbon, together with the carbide forming elements which are left in solid solution in the matrix after the first wave.

It is concluded that this second wave of precipitation is responsible for the continued hot strength of the material during cutting tool service, stabilizing a high dislocation density which may be assumed, in turn, to provide nucleation sites for the continuing precipitation process.

ACKNOWLEDGMENTS

S.K. acknowledges the support of the Alexander von Humboldt Foundation during this work. The authors are obliged to Mrs. Gaby Ketzer and Dr. Martin Silomon of the Max-Planck-Institute at Stuttgart for the measurements of hardness and resistivity shown in Figures 1 and 2.

REFERENCES

1. Wang Rong and G.L. Dunlop: *Acta Metall.*, 1984, vol. 32, pp. 1591-99.
2. H.F. Fischmeister, S. Karagöz, and H.-O. Andrén: *Acta Metall.*, 1988, vol. 36, pp. 817-25.
3. H.-O. Andrén: *Scripta Metall.*, 1981, vol. 15, pp. 749-52.
4. L.E. Svensson, P.R. Howell, H.-O. Andrén, H. Nordén, and G.L. Dunlop: *Quantitative Microanalysis with High Spatial Resolution*, The Metals Society, London, 1981, no. 277, pp. 256-61.
5. K. Stiller, L.E. Svensson, P.R. Howell, Wang Rong, H.-O. Andrén, and G.L. Dunlop: *Acta Metall.*, 1984, vol. 32, pp. 1457-67.
6. K. Stiller, S. Karagöz, H.-O. Andrén, and H. Fischmeister: *J. Phys.*, 1987, vol. 48 (C6), pp. 405-10.
7. S. Karagöz and H.F. Fischmeister: *High Speed Steels*, G. Hackl and B. Hribernik, eds., Klampfer GmbH, Weiz, Austria, 1991, pp. 41-51.
8. H.-O. Andrén: *High Speed Steels*, G. Hackl and B. Hribernik, eds., Klampfer GmbH, Weiz, Austria, 1991, pp. 392-99.
9. E.M. Trent: *Metal Cutting*, Butterworth's, London, 1984, pp. 54-80.
10. K. Kuo: *J. Iron Steel Inst.*, 1953, vol. 174, pp. 223-28.
11. K. Kuo: *J. Iron Steel Inst.*, 1956, vol. 184, pp. 258-68.

12. E. Horn: *DEW-Techn. Ber.*, 1973, vol. 13, pp. 171-79.
13. C.S. Wright and R.S. Irani: *J. Mater. Sci.*, 1984, vol. 19, pp. 3389-98.
14. J.B. Lupton, S. Murphy, and J.H. Woodhead: *Metall. Trans.*, 1972, vol. 3, pp. 2923-31.
15. A.T. Davenport and R.W.K. Honeycombe: *Met. Sci.*, 1975, vol. 9, pp. 201-08.
16. R.J. Tunney and N. Ridley: *Met. Sci.*, 1979, vol. 13, pp. 585-90.
17. T. Mukherjee, W.E. Stumpf, C.M. Sellars, and W.J.McG. Tegart: *J. Iron Steel Inst.*, 1969, vol. 207, pp. 621-31.
18. G.L. Dunlop and R.W.K. Honeycombe: *Met. Sci.*, 1978, vol. 12, pp. 367-71.
19. Wang Rong, H.-O. Andrén, H. Wisell, and G.L. Dunlop: *Acta Metall.*, 1992, in press.
20. H.F. Fischmeister, I. Liem, and S. Karagöz: *Prakt. Metallogr.*, 1987, Sonderband (special volume) 18, pp. 323-31.
21. S. Karagöz, I. Liem, E. Bischoff, and H.F. Fischmeister: *Metall. Trans. A*, 1989, vol. 20A, pp. 2695-2701.
22. H.-O. Andrén and H. Nordén: *Scand. J. Metall.*, 1979, vol. 8, pp. 147-52.
23. H.-O. Andrén: *J. Phys.*, 1986, vol. 47 (C7), pp. 483-88.
24. S. Karagöz, R. Riedl, M.R. Gregg, and H. Fischmeister: *Prakt. Metallogr.*, 1983, Sonderband (special volume) 14, pp. 369-82; English version in *The Charles Hatchett Award Papers*, The Institute of Metals, London, 1986, and CBMM, Sao Paulo, Brazil, 1986, pp. 15-19.
25. H. Fischmeister, R. Riedl, and S. Karagöz: *Metall. Trans. A*, 1989, vol. 20A, pp. 2133-48.
26. J. Golczewski and H.F. Fischmeister: *Steel Res.*, 1992, vol. 63 (8).
27. I.K. Kupalova: *Metalloved. Term. Obrab. Met.*, 1980, vol. 7, pp. 55-60.
28. T. Mukherjee: *ISI Publ. No. 126*, 1979, pp. 80-96.
29. S. Karagöz and H.-O. Andrén: *Z. Metallkd.*, 1992, vol. 83 (6).
30. H.F. Fischmeister, S. Karagöz, and G. Kompek: *Beitr. Elektronenmikr. Direktabb. Oberfl.*, 1979, vol. 12/2, pp. 71-86.
31. K. Kuo: *J. Iron Steel Inst.*, 1953, vol. 173, pp. 363-75.
32. M. Bergström: *Mater. Sci. Eng.*, 1977, vol. 27, pp. 257-69 and 271-86.
33. H. Fischmeister, S. Karagöz, E. Kudielka, and J. Püber: *Aciers Speciaux*, Circle d'Etudes des Métaux, St. Etienne, 1983, paper no. 6.
34. R.W.K. Honeycombe: *Steels—Microstructure and Properties*, Edward Arnold Ltd., London, 1981, pp. 215-22.
35. L.G. Liljestrand and A. Omsen: *Metall. Trans. A*, 1975, vol. 6A, pp. 279-86.
36. J.M. Silcock, D. Raynor, and G. Willoughby: *Met. Sci.*, 1977, vol. 11, pp. 551-62.
37. L. Lundin and H.-O. Andrén: Chalmers University of Technology, Gothonburg, private communication, 1991.
38. H.-O. Andrén, S. Karagöz, Cai Guang-Jun, L. Lundin, and H. Fischmeister: *Surf. Sci.*, 1991, pp. 246-51.